

Molecular-dynamics study of incoherent quasielastic neutron-scattering spectra of supercooled water

S.-H. Chen,¹ P. Gallo,^{1,*} F. Sciortino,² and P. Tartaglia²

¹*Department of Nuclear Engineering, Massachusetts Institute of Technology, Cambridge, Massachusetts 02139*

²*Dipartimento di Fisica and Istituto Nazionale per la Fisica della Materia, Università di Roma "La Sapienza," Piazzale Aldo Moro 2, I-00185 Roma, Italy*

(Received 7 February 1997)

A molecular-dynamics simulation of extended simple point charge water in a time interval of 1 fs to 50 ns has been performed to study the single-particle dynamics of water at supercooled temperatures. In spite of the fact that upon supercooling water progressively evolves into a more open structure locally, the single-particle dynamics is nevertheless shown to be dominated by the so-called cage effect experienced by the test particle. The slow structural relaxation of the cage at low temperatures leads to the phenomenon of slow dynamics that can only be completely studied by following the trajectories into the nanosecond range. The objective of this paper is twofold. First, we test the accuracy of various approximations used in previous analyses of spectra from incoherent quasielastic neutron-scattering experiments. Second, we explore the possibility of an alternative method of analysis of high-resolution quasielastic neutron-scattering spectra, taking into account the slow dynamics in supercooled water. The approximations tested are the decoupling of the self-intermediate scattering function into a product of rotational and translational components, the physical interpretation of the origin of the experimentally observed Debye-Waller factor, the rotational-diffusion approximation of the rotational intermediate scattering function, and the random jump diffusion approximation of the translational intermediate scattering function. Various approximations used previously for the component intermediate scattering functions are not sufficiently accurate. The reason for this is that at supercooled temperatures, due to the dominant cage effect, the conventional picture of the stochastic single-particle diffusion loses its validity. The diffusion process is then progressively controlled by the structural relaxation of the cage. [S1063-651X(97)10310-5]

PACS number(s): 61.20.Lc, 61.12.Ex, 61.20.Ja

I. INTRODUCTION

Although studies of the dynamical properties of bulk supercooled water have attracted a great interest during the past decade, the details of the microscopic motions of water molecules in supercooled temperatures are still far from being completely understood and a considerable number of very recent works are concerned with this subject [1–11]. It has been proposed that supercooling of water is terminated by a limiting temperature, which is approximately located at $T_S \sim 227$ K [12]. On approaching this point, various thermodynamic quantities show an anomalous behavior and some dynamic quantities appear to follow a power law in $|T - T_S|$ [13]. In our recent molecular-dynamics (MD) simulations on bulk supercooled extended simple point charge (SPC/E) water [14,15] we observed a power-law decrease of the diffusion coefficient and discussed the possibility of interpreting T_S as the temperature of structural arrest, called T_C in mode coupling theory (MCT) [16] of supercooled liquids. This interpretation of the limiting temperature would support the view that no thermodynamic singularity is required to explain the singular behavior of transport properties in supercooled water near T_S at low pressure [17], because MCT predicts that the transport coefficients such as the self-

diffusion constant will tend to zero and viscosity will diverge with a power law at T_C . We also carried out extensive analyses to test other predictions of MCT using our MD results. We found that many of the MCT predictions in terms of scaling relations are satisfied by supercooled SPC/E water.

Nonetheless, an experimental detection of such a behavior is not easy since bulk water at ambient pressure can be supercooled only down to approximately 235 K. By lowering T further, homogeneous nucleation has been observed to occur at approximately 10 K above T_S [18]. Although encouraging hints of an MCT-like behavior have been detected experimentally in supercooled water and discussed over the years [6,18,19], no definitive analysis in terms of the predicted behavior of quasielastic spectra has been given so far in the literature.

In this paper we will focus on the possibility of detecting a MCT-like behavior of supercooled water through quasielastic neutron scattering (QENS) experiments. QENS is a probe that has been often successfully used to test the MCT predictions in other glass-forming liquids. QENS is also a suitable probe to study the nature of diffusive motion in water [20]. For water the main contribution to the scattering cross section of neutrons comes from the incoherent part of the scattering of hydrogen atoms. The time dependence of the incoherent scattering amplitude of an atom is determined completely in terms of its single-particle motions. The double-differential neutron-scattering cross section for water is therefore directly proportional to the self-dynamic struc-

*Present address: Dipartimento di Fisica, Università di Roma "La Sapienza," Piazzale Aldo Moro 2, I-00185 Roma, Italy.

ture factor $S_H^S(Q, t)$, which is the space-time Fourier transform of the van Hove self-correlation function of the hydrogen atoms. All the correlation functions treated in this paper are related to the single-particle motions. The superscript S , meaning self, will be omitted in all that follows. Inelastic neutron scattering and QENS probe dynamics of hydrogen atoms on time scales that can be easily accessible by a MD simulation. Typically neutrons can probe dynamics ranging from fractions of a femtosecond to few tenths of a picosecond. In particular, inelastic neutron scattering covers an energy range from 0 to hundreds of meV and QENS from 0 to 2 meV. It is useful to note that 1 meV in the frequency domain corresponds approximately to 1.52 ps^{-1} .

Ever since the pioneering works of QENS on water [20,21] there have been numerous inelastic-neutron-scattering and QENS experiments on this liquid at ordinary temperatures. Among these, several works have been devoted to QENS of supercooled water up to recent years [22–24]. In the analyses of these data the authors always assumed a decoupling of rotational and translational motions of the molecules in order to have a tractable analytical model for the calculation of the intermediate scattering function $F(Q, t)$ for the hydrogen atoms. The $F_H(Q, t)$, which is the spatial Fourier transform of the Van Hove self-correlation function, was written as

$$F_H(Q, t) = e^{-Q^2 \langle u^2 \rangle / 3} R(Q, t) T(Q, t), \quad (1)$$

where the first exponential term on the right-hand side of the equation is assumed to be the Debye-Waller factor [25] originated from vibrational motions of the hydrogen atom around its equilibrium position, the second term $R(Q, t)$ represents the intermediate scattering function of the rotational motion of the hydrogen atom with respect to the center of mass of the water molecule, and the third term $T(Q, t)$ represents the intermediate scattering function of the translational motion of the center of mass. Denoting the center of mass coordinate by \mathbf{R} and the vector from the center of mass to the hydrogen atom by \mathbf{b} , the translational part of the intermediate scattering function is written as

$$T(Q, t) = \langle e^{-i\mathbf{Q} \cdot \mathbf{R}(0)} e^{i\mathbf{Q} \cdot \mathbf{R}(t)} \rangle \sim e^{-\Gamma(Q)t}. \quad (2)$$

The second equality on the right-hand side is the result of assuming an isotropic random jump-diffusion model [26] for the translational motion, where

$$\Gamma(Q) = \frac{DQ^2}{1 + DQ^2\tau_0}. \quad (3)$$

In this expression τ_0 is the residence time for the jump diffusion and D the diffusion coefficient; both can be extracted from the experimental data analysis. The rotational part of the intermediate scattering function is written as a Sears expansion [27]

$$R(Q, t) = \langle e^{-i\mathbf{Q} \cdot \mathbf{b}} e^{i\mathbf{Q} \cdot \mathbf{b}(t)} \rangle \quad (4)$$

$$= \sum_0^{\infty} (2l+1) j_l^2(Qb) C_l(t) \quad (5)$$

where the l th-order rotational correlation function is defined as

$$C_l(t) = \langle P_l(\hat{\mathbf{b}} \cdot \hat{\mathbf{b}}(t)) \rangle \quad (6)$$

and P_l is the l th order Legendre polynomial. One normally makes a diffusion approximation for the rotational-correlation function that results in

$$C_l(t) = e^{-l(l+1)D_R t}, \quad (7)$$

where D_R is the rotational-diffusion constant. This simple model contains essentially four parameters $\langle u^2 \rangle, D, \tau_0, D_R$ that can be extracted from fitting the normalized experimental data. Although this model agrees quite well with experimental data [22–24], the various approximations made have never been separately proven to be appropriate for water. On the contrary, recently several authors inferred that this picture is not valid upon supercooling [1,4,28].

In this work we take advantage of the fact that we can generate accurately the separate correlation functions by a computer simulation to explore the possibility of using MD to test individually these three major approximations, namely, the decoupling approximation (1), the jump-diffusion approximation (3), and the rotational-diffusion approximation (7). We also tackle the problem of the extent and the strength of the rotation-translational coupling as a function of the wave-vector transfer Q and temperature T . We propose, as a consequence, a different procedure for fitting QENS.

The paper is organized as follows. In Sec. II we briefly describe the details of the simulations and compare the results of the SPC/E potential known in the literature with some experimental findings in order to discuss to what extent such a potential is capable of mimicking the properties of real water. We also discuss in some detail the partial radial distribution functions $g_{\alpha\beta}(r)$ for SPC/E water, where the indices α and β can be both oxygen and hydrogen. In Sec. III we analyze in (Q, t) space those results of our MD data that can be tested with QENS. In Sec. IV we discuss the role of rotation-translation coupling and the accuracy of the rotational-diffusion approximation. In Sec. V we present the self part of the dynamic structure factor for SPC/E water down to the deeply supercooled region $S_H(Q, t)$ and discuss to what extent it can be measured with QENS. We then discuss the validity of the jump-diffusion approximation and propose a different formula for analyzing the QENS data of supercooled water. In Sec. VI we present the response function of our MD data $\chi''(Q, t)$. Finally, in Sec. VII we derive our conclusions.

II. DETAILS OF THE SIMULATION AND COMPARISON WITH MEASURED QUANTITIES FOR SPC/E

We carried out an extensive simulation of a system of 216 water molecules interacting via the SPC/E [29] potential. We studied seven temperatures, ranging from 284.5 K down to 206.3 K. For the lowest temperature we recorded water trajectories for more than 50 ns. We also studied a system of 432 SPC/E molecules forming hexagonal ice at $T = 194.0 \text{ K}$. Further details of the simulations and of the potential are given in [14,15].

Most of the existing comparisons between SPC/E water and experimental, water properties have been done at high and ambient temperatures (see, for example, [30,31]), so little is known about deep supercooled temperatures. As far as high and close to ambient temperatures are concerned, SPC/E is known to reproduce quite well the transport coefficients, i.e., shear viscosity, diffusion constant, and thermal conductivity. For example, zero-frequency shear viscosity has been calculated at both 300 and 277 K [32] and very good agreement with experimental data has been obtained at both temperatures.

As far as the supercooled results are concerned, from studies carried out for temperatures between 235 K and 330 K at a pressure of 1 bar the diffusivity is reported to coincide with experimental data in water at approximately 275 K [33]. The values obtained from MD are slightly smaller than that from the experiment for higher temperatures but become increasingly larger for lower T until 240 K. Also the heat capacity from MD is found to be larger than that from the experiment for low temperatures by the same authors.

SPC/E is also capable of reproducing the pressure-dependent temperature of maximum density [33–35]. In spite of the displacement of the MD phase diagram from the phase diagram of real water, this potential has also been used recently to produce MD data in agreement with experimental QENS data for temperature down to 264 K [1].

We now compare the results of our simulation for the radial distribution function $g_{\alpha\beta}(r)$ with the experiments on water and hexagonal ice. A determination of $g_{\alpha\beta}(r)$ through combination of different diffraction experiments is by no means a straightforward task, so very few reliable determinations are available. One of the most accurate works at ambient temperature is done by Soper [36]. In the top portion of Fig. 1, experimental data for $T=298$ K at ambient pressure from Ref. [36] are shown together with our MD results for $g_{OO}(r)$, $g_{OH}(r)$, and $g_{HH}(r)$ at $T=284.5$ K. Soper calculated the coordination number of the first peak of $g_{HH}(r)$ to be 5.8 ± 0.3 at $T=298$ K and we obtain approximately 5.1 for SPC/E water at $T=284.5$ K. We can see that around room temperature the $g_{\alpha\beta}(r)$ are reproduced quite well by SPC/E potential. It is also worth noting that in their original paper Berendsen *et al.* [29] compared SPC/E results at 306 K to the $g_{OO}(r)$ extracted from experimental data of Thiessen and Narten at $T=298$ K [37]. This determination is less accurate than Soper's result. The agreement of SPC/E $g_{\alpha\beta}(r)$ with experiment is indeed much better with Soper's data as far as the height of the first peak is concerned. Nevertheless, the first SPC/E peak of $g_{OO}(r)$ is still situated much too inward and it is too sharp compared to the experimental one because of the r^{12} repulsive term contained in the potential [29].

The results of our simulations of $g_{\alpha\beta}(r)$ for hexagonal ice are also shown in Fig. 1, bottom, for comparison with that of the supercooled water. In the three graphs, $g_{OO}(r)$, $g_{OH}(r)$, and $g_{HH}(r)$, respectively, are shown. The first and second peaks in ice always coincide with that of the supercooled water but are sharper and after the second peak there is no longer a one to one correspondence. The $g_{\alpha\beta}(r)$ for ice have been calculated by averaging over all the possible directions in order to compare it with the homogeneous $g_{\alpha\beta}(r)$ of supercooled water. We also observe by looking at the $g_{\alpha\beta}(r)$

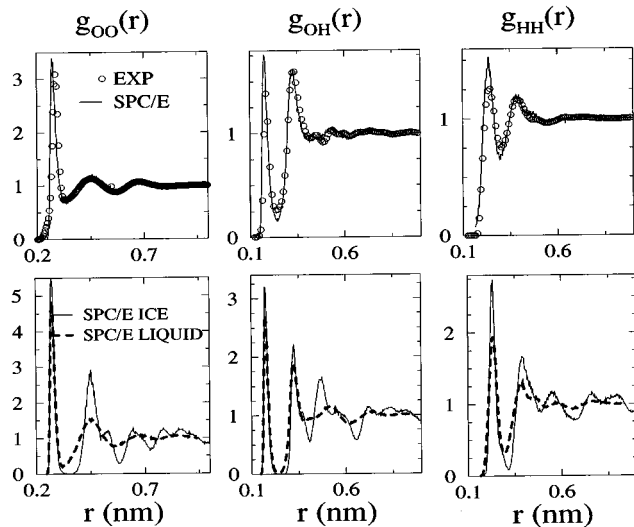


FIG. 1. Three partial radial distribution functions of water. On the top our MD data at $T=284.5$ K (continuous line) are presented together with experimental data from Ref. [36] at $T=298$ K and ambient pressure (circles). On the bottom the radial distribution functions of MD water at $T=206.3$ K (thick dashed) are presented together with the radial distribution function for hexagonal ice (continuous). In order to make a comparison with water the radial distribution functions of ice have been calculated, averaging over all the directions.

of SPC/E water at $T=284.5$ and 206.5 K, top and bottom, respectively, that peaks become sharper and increase in height as temperature decreases, indicating that the nearest-neighbor and next-nearest-neighbor shells become more well defined on supercooling.

III. SPC/E WATER AND THE KINETIC GLASS TRANSITION

The analyses of the single-particle dynamics of the oxygen motion of water molecules of our MD simulations in time domain have been reported in two previous papers [14,15]. As stated in the Introduction, we found clear evidence that SPC/E water undergoes a kinetic glass transition, at about 50 K below the temperature of maximum density. Since T_S for real water is estimated to be approximately 49 K below the temperature of maximum density, we suggested the interpretation of T_S as the crossover temperature of MCT for the dynamic glass transition T_C [38].

In the following we will briefly summarize the results of our two previous studies [14,15] and then go on to analyze intermediate scattering function of the hydrogen atoms. Since QENS on water probes the single-particle dynamics of hydrogen atoms we will show that the time evolution of correlation functions related to hydrogen motion is very similar to that of oxygen atoms (or of the center of mass), except for very early times, i.e., for high frequencies that are definitely beyond the range of QENS measurement. The results we found for the oxygen atoms [14,15] can thus be applied directly to QENS study. This is a significant finding as far as the analysis of experimental results is concerned.

In many fragile glass-forming liquids, it has been observed that, on supercooling, or on increasing the density,

each molecule or atom experiences an increased degree of confinement in a potential well, called a cage, created by its neighbors. The confinement within the cage manifests itself as a plateau in the time dependence of the mean-square deviation in the intermediate-time range. In fact, once the cage begins to form in the liquid, the test particle remains trapped in the cage for longer and longer times as the liquid approaches T_C . More specifically, the relaxation of the test particle intermediate scattering function in (Q, t) space evolves from a single exponential decay typical of a liquid behavior to a two-step process typical of a glasslike behavior. In the vicinity of T_C the correlation function decays initially fast to a plateau value (this region is called a β regime), after which it decays slowly to zero (an α regime).

MCT describes satisfactorily the shape of the relaxation function. In MCT, the approach to the plateau is described by a power law in time with an exponent a and the departure by a power law with another exponent b . This is called the von Schweidler law [39]. The α decay is well described by a stretched exponential $e^{-(t/\tau)^\beta}$. τ represents the characteristic time for structural relaxation and diverges on approaching T_C with a power γ . The inverse of the diffusion coefficient is predicted to diverge with the same exponent γ . For MCT a , b , and γ are related so that only one of these exponents is independent. This means that within this theory the α - and β -relaxation processes are closely connected. For further details see, for example, Ref. [39].

Through the analysis of oxygen motion we found that dynamics of SPC/E supercooled water is characterized by a fast and a slow relaxation process. Moreover, we detected the presence of a time region in which dynamics is self-similar in time. In this region, the intermediate scattering function decays as a power law whose range of validity is r dependent. The range of validity of the von Schweidler law is maximum for distances close to the first-neighbor shell or Q values close to the maximum of $S(Q)$. In the late-time region the intermediate scattering function decays as a stretched exponential. The value of the stretching exponent β is T and Q dependent. The relaxation times diverge at small Q as a power law with an exponent γ that is the same as that of the diffusion coefficient. Furthermore, the relation between γ and the exponent b , calculated in the self-similar β relaxation region, is in agreement with MCT predictions.

We now discuss the incoherent $F(Q, t)$ for hydrogen atoms,

$$F_H(Q, t) = \langle e^{-i\mathbf{Q} \cdot [\mathbf{r}_H(t) - \mathbf{r}_H(0)]} \rangle, \quad (8)$$

where the angular brackets denote the ensemble average and $\mathbf{r}_H(t)$ and $\mathbf{r}_H(0)$ are, respectively, the coordinate of a hydrogen atom at time t and the coordinate of the same hydrogen atom at time 0. This quantity is of particular interest in our analysis since the time Fourier transform of this function can be directly measured with a QENS experiment. The right-hand side of Eq. (8) can be straightforwardly evaluated from the MD trajectories. In Fig. 2 we show $F_H(Q, t)$ for all the seven temperature investigated at the first peak of $g_{OO}(r)$, $Q_{max} = 1.8 \text{ \AA}^{-1}$. For the second lowest temperature error bars are displayed together with the curve. We note that the magnitude of the errors is not significant in the simulations. In the inset the early times of the curves are sketched to-

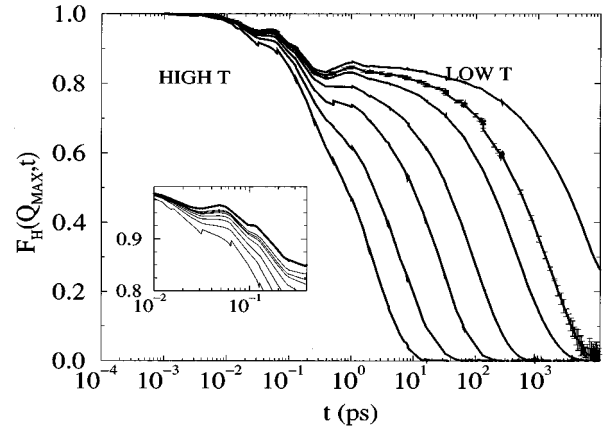


FIG. 2. Semilogarithmic plot of $F(Q, t)$ of hydrogen atoms for all the temperatures investigated at Q_{max} . The error bars are shown only for one temperature for clarity. Lower T are on the top. In the inset only the early times are shown for all the temperatures and for hexagonal ice (thick line) at $T = 194 \text{ K}$ along a selected Q direction at Q_{max} . Early ice features are only slightly sensitive to the Q direction. After $Q = 0.2 \text{ ps}$ ice displays an oscillating behavior, vibrational contributions, around an asymptotic value due to the absence of diffusion.

gether with the early times for ice. In Fig. 3 we show $F_H(Q, t)$ at $T = 213.6 \text{ K}$ for integer multiples of $Q = 0.33 \text{ \AA}^{-1}$. In the inset $F_H(Q, t)$ and $F_O(Q, t)$ are shown for $Q = 3 \text{ \AA}^{-1}$. Figure 2 shows that as temperature goes down, $F_H(Q, t)$ begins to develop a plateau, as we already found for the oxygen atoms in the analysis of Ref. [14,15]; see, for example, Fig. 2 of Ref. [14]. The behavior of the oxygen correlator $F_O(Q, t)$ with the existence of a plateau developing under supercooling can be observed also in the inset of Fig. 3, top curve. The early part of the hydrogen dynamics in water upon supercooling for $t < 0.2 \text{ ps}$ is similar to the dynamics in the ordered solid. In fact, we see that the hydrogen dynamics in hexagonal ice (thick curve in the inset of Fig. 2) displays the same features. The first light shoulder occurring around 0.05 ps and the second around 0.1 ps are signatures of the Q -dependent hydrogen atom libration [40]. Hence-

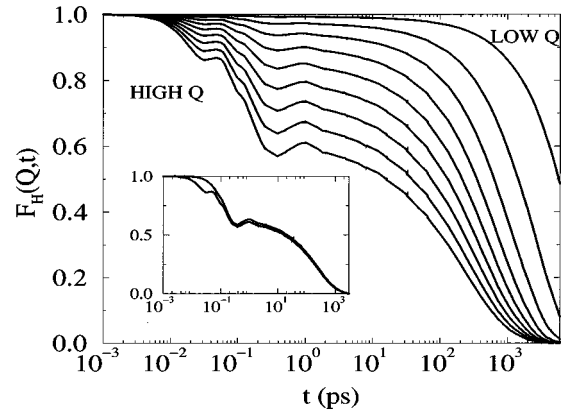


FIG. 3. Semilogarithmic plot of $F(Q, t)$ for hydrogen atoms at $T = 213.6 \text{ K}$ for integer multiples of 0.33 \AA^{-1} . Curves on the top correspond to lower Q . In the inset both hydrogen and oxygen $F(Q, t)$ are shown at the highest calculated Q , 3 \AA^{-1} , where all the features that distinguish the two curves are more evident.

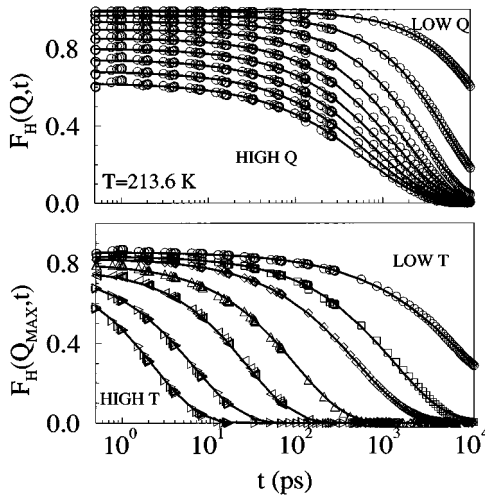


FIG. 4. Late β region of $F(Q,t)$ of hydrogen atoms. The continuous line corresponds to the fit to a stretched exponential and symbols to MD data. On the top graph integer multiples of $Q=0.33 \text{ \AA}^{-1}$ at $T=213.6 \text{ K}$ are shown. On the bottom graph all the temperatures at Q_{max} are shown.

forth the early dynamics of hydrogen is of no interest in this context since it does not display any relaxation feature that is peculiar to the supercooled state. This confines our interest only to the quasielastic region of neutron scattering. We also see from the inset of Fig. 3 that the dynamics of the oxygen atom of a water molecule is indeed very similar to that of hydrogen, except for early times, as already mentioned.

The hydrogen relaxation function for times longer than 0.2 ps shows, as the initial feature, a small bump centered around 1 ps, which has been associated with a significant harmonicity in the dynamics at short times [41–43]. This point has been discussed recently in Ref. [44].

For longer times we clearly see the α -relaxation region. Also for hydrogen, the late part of the α -relaxation region can be fitted by a stretched exponential function. The quality of the fits is shown in Fig. 4 together with MD data. The top graph shows the results at $T=213.6 \text{ K}$ for several Q values that are integer multiples of $Q=0.33 \text{ \AA}^{-1}$. The bottom graph shows the fits at Q_{max} for all the investigated temperatures ranging from $T=207.3$, to 284.5 K . As for oxygen or, equivalently, the center of mass, we see that the slow relaxation is very well represented by a stretched exponential. The values of $1/\tau$ extracted from the fits to the stretched exponential for hydrogen are reported in Fig. 5 as a function of Q^2 , together with the values extracted from the similar fits performed on the center of mass. In Fig. 6 the exponents β obtained from the fits are shown for both hydrogen and the center of mass. As we can see from the comparisons shown in Figs. 2–6, $F_H(Q,t)$ displays the same type of dynamical behavior as $T(Q,t)$ except for the early times; i.e., $t < 0.2 \text{ ps}$. The τ values associated with the α relaxation of $F_H(Q,t)$, though slightly different, show the same trend in Q , i.e., the same Q^2 to Q crossover. This same behavior had been found already for the oxygen relaxation times; see Fig. 3 of [14]. It is not surprising that oxygen atoms behave like the center of mass since their positions are almost coincident, while it is much more interesting that the center of mass, or oxygen, and hydrogen behave in the same way. Furthermore, also the

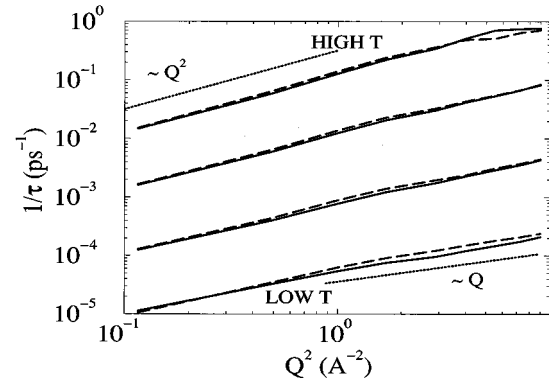


FIG. 5. A log-log plot of the inverse of τ versus Q^2 . The τ values are extracted from the fit of the late α region to a stretched exponential. Dashed lines are for hydrogen and continuous lines are for the center of mass of the water molecule. The values of the temperature are, starting from the top, $T=284.5$, 238.2 , 213.6 , and 206.3 K . The two dotted lines on the top and on the bottom of the figure, respectively, indicate the Q^2 and Q behaviors.

values of the stretch exponent β for hydrogen and the center of mass are the same. Both τ and β , as we shall see in the following paragraphs, can be measured by QENS as a function of T and Q so that the possible existence of this crossover in τ can be tested.

Obviously, the reliability of our MD data, as far as a comparison with experiment is concerned, depends crucially on the ability of the SPC/E potential to mimic the detailed characteristics of the pair-correlation functions. In particular, the agreement in the positions and heights of the peaks associated with the nearest neighbors is important since in the MCT static pair-correlation functions alone are responsible for the dynamic behavior. The good agreement of the pair-correlation functions generated from the SPC/E water with a neutron-diffraction experiment close to room temperature (shown in Fig. 1), some experimental evidence of a MCT-like behavior in supercooled water [6,18], and the recent comparison of QENS results with that of the SPC/E water

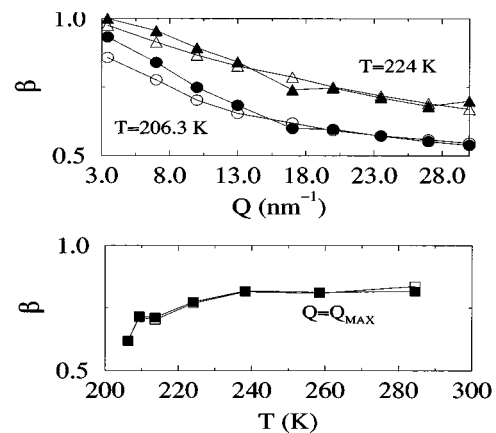


FIG. 6. Values of the exponent β extracted from the fit of the late α region to a stretched exponential. Open symbols refer to hydrogen, full symbols to the center of mass. On the top β is shown as a function of Q . Triangles refer to 224.0 K and circles refer to $T=206.3 \text{ K}$. On the bottom β is shown as a function of T at Q_{max} (squares).

[1] are encouraging. On the other hand, it is also true that the temperature of maximum density is quite different for SPC/E water and experimental water and dynamics might be sensitive to that. In addition, the SPC/E values of γ show a different behavior in pressure from that of the experimental values [18], although in different pressure ranges, in particular, $\gamma_{SPC/E}=2.29$ for $P=0.1$ MPa and $\gamma_{SPC/E}=2.73$ for $P=-80$ MPa [14], while the analysis of experimental data gives $\gamma_{expt}=1.81$ for $P=0.1$ MPa and $\gamma_{expt}=2.19$ for $P=100$ MPa [18].

It would be very important in the near future to establish the reliability of SPC/E potential in representing the dynamics of real water on supercooling since different potentials suggest different dynamical behavior on supercooling [4]. A careful high-resolution QENS study on supercooled water testing the MCT predictions would therefore be very timely.

IV. QENS AND THE ROTATION TRANSLATIONAL COUPLING

We now tackle a very important issue connected with the interpretation of QENS on water, namely, the rotation translational coupling. Since the SPC/E potential is for rigid water molecules, the vibrational motion of hydrogen atoms is absent. Therefore, in principle, there is no vibrational Debye-Waller factor present in $F_H(Q,t)$. In this case $F_H(Q,t)$ consists of translations of the center of mass and rotation of the hydrogen atoms around the center of mass alone. In order to properly analyze QENS spectra of supercooled water it is essential to understand to what extent the coupling between rotation and translation can be neglected in the computation of $F(Q,t)$ of the hydrogen motions. In the Introduction, we recalled that traditionally analyses of QENS spectra have been done assuming no coupling between the rotational and translational motion so that $F_H(Q,t)$ is the product of the translational and rotational intermediate scattering functions. If we decompose the hydrogen atom position vector into the sum of the position vector of the center of mass \mathbf{R} plus the position of the hydrogen from the center of mass \mathbf{b} , $\mathbf{r}_H=\mathbf{R}+\mathbf{b}$, then the decoupling assumption for a rigid molecule states

$$F_H(Q,t) \approx T(Q,t)R(Q,t), \quad (9)$$

where $T(Q,t)$ and $R(Q,t)$ are defined in Eqs. (2) and (5), respectively. All these three correlation functions can be easily calculated separately by MD. We can therefore make an estimate on how good this decoupling approximation is for SPC/E water as a function of Q and T .

When dealing with a correlation function that is a product of several terms, each one with a (Q,t) dependence, it is always possible to rewrite it as the sum of all the possible factorizations of its terms plus another irreducible term, which we shall call the connected intermediate scattering function $F_{con}(Q,t)$. $F_{con}(Q,t)$ contains the contribution coming from the four factors coupled together in the correlation function and generally speaking it is different from zero. This procedure is applicable also to our correlation function. In fact, $F_H(Q,t)$ is the product of four exponential functions

$$F_H(Q,t) = \langle e^{-i\mathbf{Q}\cdot\mathbf{R}(0)} e^{-i\mathbf{Q}\cdot\mathbf{b}(0)} e^{i\mathbf{Q}\cdot\mathbf{R}(t)} e^{i\mathbf{Q}\cdot\mathbf{b}(t)} \rangle. \quad (10)$$

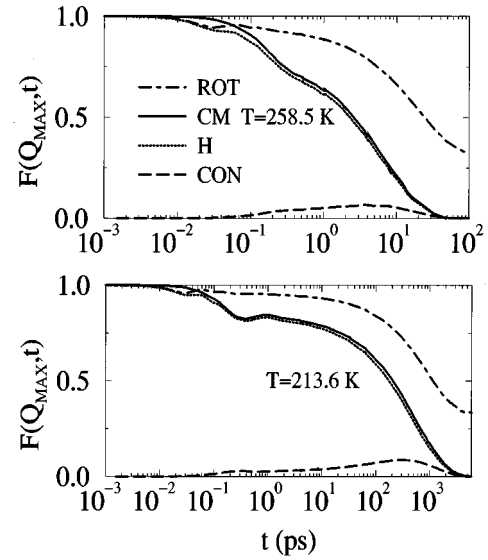


FIG. 7. Starting from the top curve in the graphs, semilogarithmic plot of $R(Q,t)$, $T(Q,t)$, $F_H(Q,t)$, and the connected correlation function $F_{con}(Q,t)$ at Q_{max} . The top graph represents $T=258.5$ K and the bottom graph $T=213.6$ K.

Equation (10) can be rewritten as

$$\begin{aligned} F_H(Q,t) - F_{CON}(Q,t) &= \langle e^{-i\mathbf{Q}\cdot\mathbf{R}(0)} e^{i\mathbf{Q}\cdot\mathbf{R}(t)} \rangle \\ &\quad \times \langle e^{-i\mathbf{Q}\cdot\mathbf{b}(0)} e^{i\mathbf{Q}\cdot\mathbf{b}(t)} \rangle \\ &\quad + \langle e^{-i\mathbf{Q}\cdot\mathbf{R}(0)} e^{i\mathbf{Q}\cdot\mathbf{b}(t)} \rangle \\ &\quad \times \langle e^{i\mathbf{Q}\cdot\mathbf{R}(t)} e^{-i\mathbf{Q}\cdot\mathbf{b}(0)} \rangle. \end{aligned} \quad (11)$$

The contributions arising from all the terms composed of products of \mathbf{R} and \mathbf{b} variables at arbitrary time are zero on average, due to the statistical independence between the two [45]. Therefore, the following relation holds:

$$F_{con}(Q,t) = F_H(Q,t) - T(Q,t)R(Q,t). \quad (12)$$

$F_{con}(Q,t)$ describes the strength of the coupling between translational and rotational motions as a function of Q and t as observable by QENS. In the graphs of Figs. 7 and 8 we show on a semilogarithmic scale $R(Q,t)$, $T(Q,t)$, $F_H(Q,t)$, and $F_{con}(Q,t)$. In Fig. 7 these functions are shown for two temperatures at Q_{max} . In Fig. 8, for the same two temperatures on the corresponding graphs, we show the four correlation functions calculated for $Q=0.33 \text{ \AA}^{-1}$. These Q values are also quite close to the maximum and the minimum Q value that can be probed by a typical QENS experiment. We see that the rotational correlation function $R(Q,t)$ has as expected, the same short-time features of $F_H(Q,t)$ and decays to a nonzero constant value, due to the fact that the motion of hydrogen, as seen from the center of mass, is confined into a spherical volume of radius b [see Eq. (5)]. $R(Q,t)$ bears no evident signatures of the small bump observed around 1 ps in $F(Q,t)$ and in $T(Q,t)$ (see the bottom curve of Fig. 7 for $T=213.6$ K at Q_{max}). We also observe that $F_{con}(Q,t)$ is non-negligible for Q close to Q_{max} , meaning that there is a visible coupling between rotational and translational motion at large Q . At Q_{max} the rotational func-

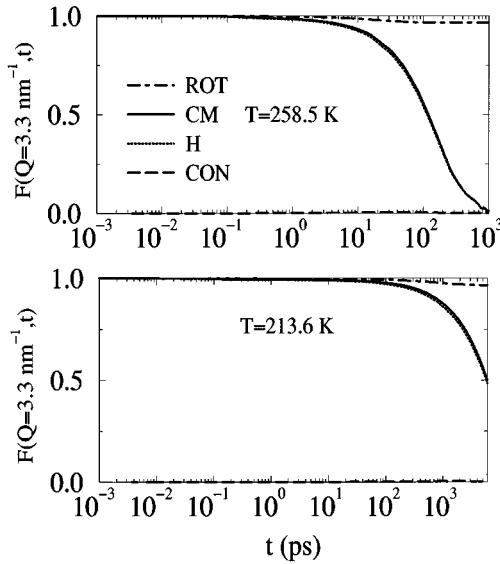


FIG. 8. Same as in Fig. 7 at a lower wave vector $Q=0.33 \text{ \AA}^{-1}$. It is evident that for this Q value the coupling is practically absent.

tion decays to its constant value on the same time scale as the center of mass and hydrogen. For $Q=0.33 \text{ \AA}^{-1}$ the coupling is negligible and we observe that the rotational correlation function decays very slowly and for the top curve of Fig. 8 is still practically one when $T(Q,t)$ and $F_H(Q,t)$ have already decayed to zero. In order to get a better understanding of the coupling behavior as a function of time we also plotted in Figs. 9 and 10 $F_{con}(Q,t)$ as a function of T at Q_{max} and as a function of Q at $T=213.6 \text{ K}$, respectively. It is interesting to note that there is a feature in $F_{con}(Q,t)$ appearing in the same region of the bump. The strength of the translational-rotational coupling shows in fact a bump at 0.26 ps, the same time of the first minimum in $F(Q,t)$ of

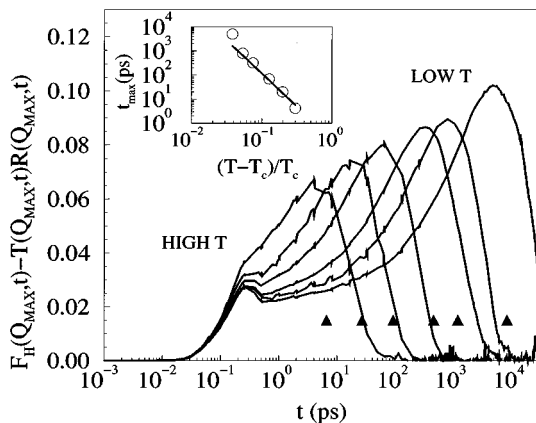


FIG. 9. Semilogarithmic plot of $F_{con}(Q,t)$ vs t for hydrogen atoms at Q_{max} . Different curves correspond to different temperatures. Curves on the left correspond to higher T and we show all the T of our MD on water except the highest, where the statistics was poorer. The arrows in the bottom of the figure mark the relaxation times of the hydrogens for different T at Q_{max} . Shown in the inset is a log-log plot of the maximum of $F_{con}(Q,t)$ as a function of $(T-T_c)/T_c$ (circles). The straight line is a power law with exponent 2.73 and $T_c=198.7 \text{ K}$.

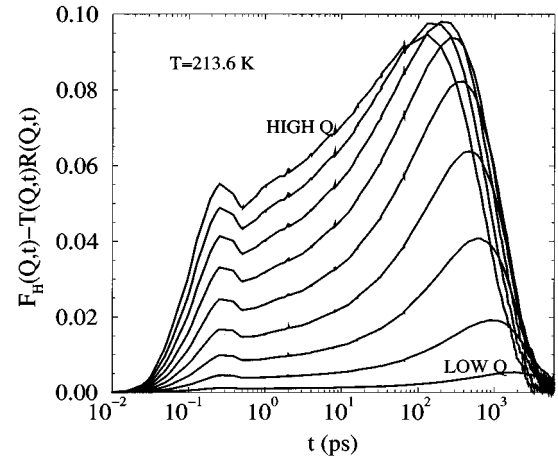


FIG. 10. $F_{con}(Q,t)$ vs t at $T=213.6 \text{ K}$ as a function of Q for the first nine integer multiples of 0.33 \AA^{-1} . The correlation function grows with Q .

hydrogen and oxygen. The bump becomes more and more evident as Q grows and does not shift with T and Q . After this bump the coupling continues to increase until it reaches a peak and eventually decays to zero.

Both the height and the position of the second peak shift with temperature and Q vectors. We recognize clear signatures of the cage effect also in this coupling. In our previous work we already discussed the time evolution of the first two angular correlation functions $C_1(t)$ and $C_2(t)$ that appear in Eqs. (5) and (6) and we observed [46] that the breaking and reforming of cages is the bottleneck of both rotational and translational diffusion. We see here that indeed, as we cool down the system $F_{con}(Q,t)$ is mastered by the dynamics of the molecules. This correlator describes the strength of the coupling between translation and rotation and increases very slowly in the region of the plateau of $F_H(Q,t)$, that is, in the region where the hydrogen atoms are trapped in the cage, and successively reaches its height for a time close to the cage relaxation time. This means that as the cages relax, molecules are free to move and rotate and translation and rotational motions also begin to decouple. On the bottom of Fig. 9 the hydrogen relaxation times are marked with triangles as a function of T . We note that they are close to the peak positions. In the inset of Fig. 9 the circles represent the positions of the maximum of $F_{con}(Q,t)$ as a function of $T/T_c - 1$ at Q_{max} and the line is a power law with exponent 2.73 and $T_c=198.7 \text{ K}$, i.e., the same values found studying the power-law behavior of D [14]. It is very interesting that, except for the lowest temperature, the peak positions scales with the same γ of D and the τ associated with the late part of the α relaxation. This confirms that, as predicted by the MCT, it is the cage effect that masters the dynamic behavior of this system, including the behavior of the correlator that describes the rotation-translational coupling $F_{con}(Q,t)$.

From our analysis it also appears that the coupling is very weak for low- Q values where $R(Q,t)$ remains close to one for long time. Since that is the range of Q where most high-resolution QENS has been performed, so far it is an acceptable approximation to decouple rotational and translational degrees of freedom. But we note that the coupling is never decaying on a faster time scale; on the contrary it remains

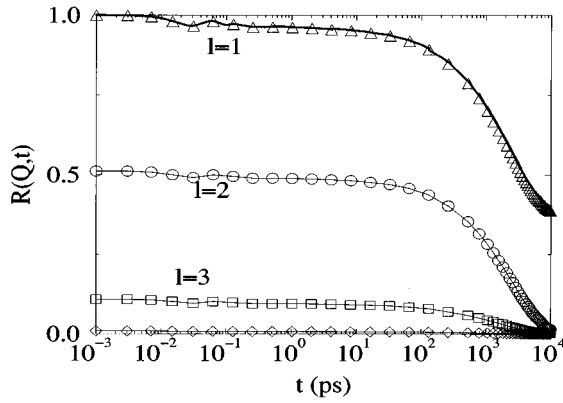


FIG. 11. $R(Q,t)$ for $T=209.3$ K and $Q=1.7 \text{ \AA}^{-1}$ calculated exactly from our MD data (thick line) and as a sum of the first four terms of the Sears expansion (triangles). In the same graph we also report separately the contribution of the $l=1$, $l=2$ (squares), and $l=3$ (diamonds) terms.

different from zero over the whole range spanned by the various $F(Q,t)$. Thus, at low Q we do not expect to detect any rotational signature in QENS. Close to Q_{max} , the coupling is already significantly enhanced. The relative strength of its contribution to the total $F(Q,t)$ remains more or less constant over the whole T range for corresponding Q .

We next analyze the validity of the rotational diffusion approximation. Since in water the magnitude of the b vector appearing in Eq. (5) is very close to 1 \AA (0.9461 \AA for SPC/E), for the Q range less than 2 \AA^{-1} , the only significant contribution to the rotational-correlation function in the Sears expansion (5) comes from the first three terms. The first term is independent of t , so in practice only the behavior of the first two orders of the rotational-correlation function $C_1(t)$ and $C_2(t)$ are needed to construct the total rotational intermediate scattering function. We illustrate this point in Fig. 11 for $Q=1.7 \text{ \AA}^{-1}$. The top curve of Fig. 11 is the MD result for $R(Q,t)$. Triangles are the sum of the first four terms of the Sears expansion. Circles, squares, and diamonds are, respectively, the $l=1$, $l=2$, and $l=3$ contributions. We see that the $l=3$ term is still not giving any contribution close to Q_{max} of water. As far as the decay of the various orders of the rotational-correlation function is concerned, we show [46] that they are fitted by a stretched exponential for low T and Q close to Q_{max} , so that the range of validity of the rotational-diffusion approximation is confined to the low- Q region for the lower temperatures. At room temperature $\beta \rightarrow 1$ and the rotational diffusion approximation could be accepted for the entire Q range in which β is close to 1. But, unfortunately, in the high- Q region the decoupling approximation is no longer valid also for quite high temperatures.

V. THE DYNAMIC STRUCTURE FACTOR: QENS TEST OF MCT

We will now concentrate on the study of hydrogen single-particle motions in (Q,ω) space as probed by QENS, for a MCT test. Since we showed in Sec. III that the long-time behavior of hydrogen is similar to that of the center of mass, apart from minor differences, we conclude that in the high-resolution QENS experiment on supercooled water the line

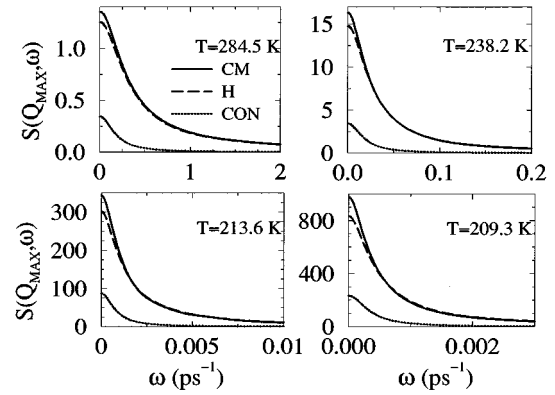


FIG. 12. Starting from the top of each figure, the curves represent the Fourier transform of the fit to the intermediate scattering functions of the center of mass and the hydrogen atoms and the direct Fourier transform of the connected correlation contribution. The Q value is Q_{max} . The top-left figure is for $T=284.5$ K, top-right for $T=238.2$ K, bottom-left for $T=213.6$ K, and bottom-right for $T=209.3$ K. $1 \text{ meV} \approx 1.52 \text{ ps}^{-1}$.

shape at the quasielastic region is essentially given by the center of mass motion only, for the whole Q range. A similar conclusion is presented in Ref. [1].

We also showed that the coupling of rotation and translation is in general non-negligible at all the investigated T for high- Q values. In order to give a more quantitative estimate of its weight in the Fourier transform we show in Fig. 12 the time Fourier transform of $T(Q,t)$, $F_H(Q,t)$, and $F_{con}(Q,t)$ for different temperatures at Q_{max} . We see that the difference between the center of mass and the hydrogen is not as big as the contribution coming from $F_{con}(Q,t)$ in the frequency space. We therefore must deduce that the effect of the rotational-translation coupling and the decay of the rotational correlation tend to cancel each other in the high- Q region in such a way that, in spite of the non-negligible coupling, $F_H(Q,t) \approx T(Q,t)$ in the entire long-time region for the entire Q range. In Fig. 13 we show the time Fourier transform of $F_H(Q,t)$ and $F_{con}(Q,t)$ for $Q=0.3 \text{ \AA}^{-1}$. In this region the rotational-translational coupling is negligible, as expected since the rotational-function remains close to 1 for almost the entire time (see Fig. 8).

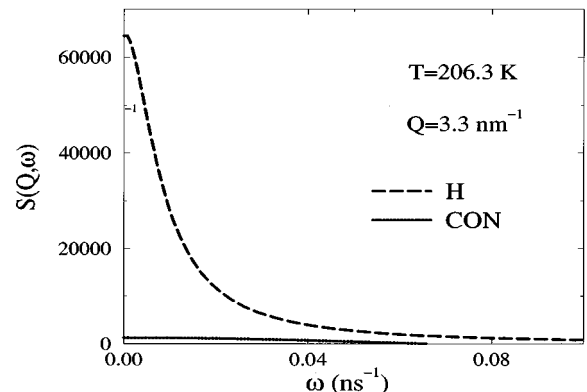


FIG. 13. Same as in Fig. 12 for $Q=0.3 \text{ \AA}^{-1}$ and $T=206.3$ K. We observe that the coupling between translation and rotation is negligible here.

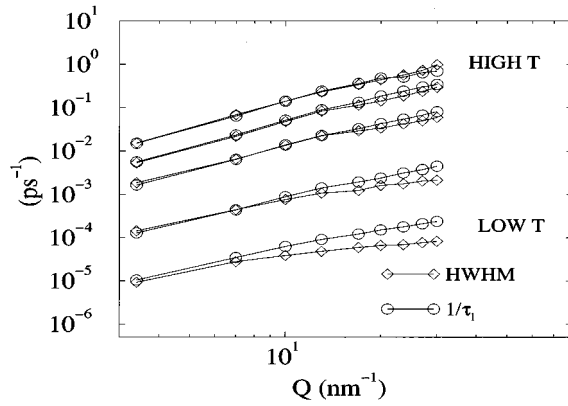


FIG. 14. Diamonds represent the full width at half maximum of the $S_H(Q, \omega)$ as a function of Q for different temperatures. Circles represent the values of τ extracted from the fit of the late α region to a stretched exponential. We see, as expected, that these values become more and more different as Q grows and T decreases, i.e., as the exponential of the long-time relaxation becomes more and more stretched.

In analyzing the experimental data the QENS line shape can therefore be fitted to a stretched exponential whose strength factor is called the Lamb-Mössbauer factor and the $1/\tau$ extracted from the analysis of the line shape can be considered, with a very good degree of accuracy, the relaxation time for structural relaxation at the selected Q vector.

We now compare our results with those that have been obtained in the past by using the jump-diffusion model for the analysis of the data. In the jump-diffusion model the half-width at half maximum (HWHM) Γ is directly connected to the relaxation time. This is a consequence of the fact that the line shape of the quasielastic peak is Lorentzian. Traditionally, Γ is therefore plotted as a function of Q at different temperatures. It is well known that for jump diffusion to hold this quantity has to display a saturation for Q values that ranges approximately from 1 to 1.7 \AA^{-1} for experimental water at ambient pressure and T ranging from 20 °C down to -20 °C [22,23]. In Fig. 14 we show both the HWHM extracted from the $S_H(Q, \omega)$ of our MD data (diamonds) and the τ values that can be extracted from the fit of the line shape to the stretched exponential (circles). We recognize that as the value of β decreases from 1 down to approximately 0.6 (it does so with decreasing temperature and increasing Q , as we showed in Fig. 6) the inverse of the relaxation time becomes more and more different from the HWHM. We also observe that the $1/\tau$ versus Q plot does not saturate at large Q and low T , indicating that the simple jump-diffusion model is not valid for SPC/E water when supercooled. At the same time the HWHM of the MD data shows saturation, which might be the one observed experimentally. This saturation has neither an analytical nor a numerical relation with the τ alone for SPC/E water since also β is changing. Therefore, it is of no physical interest for QENS analysis of supercooled water provided it behaves like SPC/E water.

As far as the QENS analysis of the rotational function is concerned, when it can be decoupled from the translational one, i.e., for low Q , the line shape is not sensitive to the rotational correlation function. This is the typical range of Q

that we have observed in QENS so far. In testing MCT around Q_{max} these contributions cannot instead be considered separately. But also in this case there will be no detectable signatures of the rotational motion in QENS since for long times $F_H(Q, t) \sim T(Q, t)$. In fact, we showed that $F_H(Q, t)$, $T(Q, t)$, and $R(Q, t)$ decay on the same time scale so they cannot be decoupled according to the “old” data analysis, and the rotational decay is very weak, so it bears no distinct signatures in the Fourier transform of the $F_H(Q, t)$.

In our previous analysis [14,15] we fitted $F_O(Q, t)$ with the sum of a Gaussian contribution plus a stretched exponential

$$F(Q, t) = [1 - A(Q)]e^{-(t/\tau_s)^2} + [A(Q)]e^{-(t/\tau_l)^\beta}, \quad (13)$$

see, for example, Fig. 2 of [14]. The Gaussian part accounts for all the processes that take place on a fast time scale, while the stretched exponential allows a detailed analysis of the late α relaxation [47]. Referring to MCT, it is important to stress here that Eq. (13) is a phenomenological formula that does not allow one to study either the approach to or the departure from the plateau, i.e., it does not allow one to verify the possible existence in water of the two power-law regions of MCT characterized by the exponents a and b and their connection. The value of the exponent b can be determined by a careful analysis of the behavior of $F(Q, t)$ [or from its measurable analog $S(Q, \omega)$] in the α -relaxation regime. We did show (see Figs. 7 and 13 of Ref. [15]) that the range of validity of the power-law region characterized by b is very limited. As regards the range of validity of the approach to the plateau characterized by the exponent a , we cannot make precise statements since in our simulation it is completely covered by the microscopic dynamics, clearly visible in the oscillation around 0.2–0.3 ps in all the $F(Q, t)$; see, for example, the inset in Fig. 2. So the Gaussian form of the fast relaxation is only an approximation for the well-known experimental feature of the short-time behavior of water. The details of this behavior do not concern the present study since it is beyond the QENS range, but the inclusion of the Gaussian term in the formula ensures the proper normalization of the fit to the QENS spectra. We therefore propose that the Fourier transform of this expression can be used also to fit QENS experimental data. In fact, we did show in Sec. III that in the QENS range the dynamics of the center of mass, of oxygen, and of hydrogen are very much the same and we showed in our previous papers [14,15] that Eq. (13) is a very good equation to fit $F_O(Q, t)$; see, for example, Fig. 2 of Ref. [14]. The Gaussian term can be Fourier transformed analytically. Under certain conditions, the Fourier transform of the stretched exponential can be approximated with the Cole-Cole or the Cole-Davinson function. This data analysis would allow one to calculate both τ_l and β .

Our simulation has been performed with rigid molecules so that the Debye-Waller factor appearing in Eq. (1) is equal to one [25]. Still, performing the fit, we do observe a Q -dependent attenuation factor, $A(Q)$ of Eq. (13), in the intermediate scattering function at a long time. We identify this factor with the nonergodicity parameter or Lamb-Mössbauer factor of MCT. The term “nonergodicity parameter” is due to the fact that this parameter allows one to

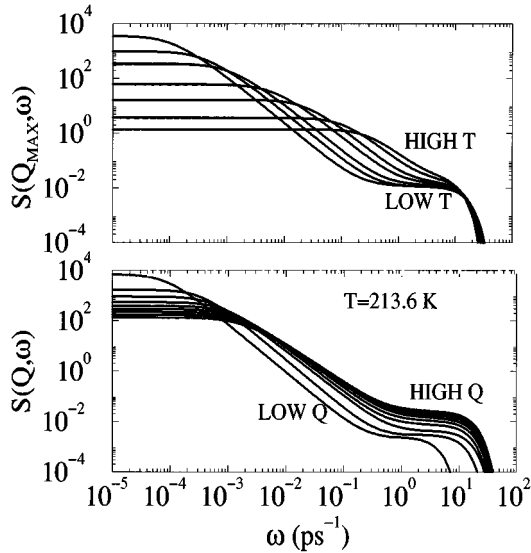


FIG. 15. Behavior of $S(Q, \omega)$ on the top as a function of temperature at Q_{max} and on the bottom as a function Q for $T=213.6$ K. The curves have been obtained by a Fourier transform of Eq. (13).

determine the ergodic to nonergodic transition occurring at T_C in MCT. At T_C , in fact, MCT predicts

$$F(Q, t \rightarrow \infty) = A(Q), \quad 0 < A(Q) < 1. \quad (14)$$

This equation means that perturbations of the system do not relax to zero; therefore, the system behaves nonergodically [48]. In our simulations (all performed above T_c) the system is ergodic and the behavior of $A(Q)$ as a function of temperature can only be inferred by the behavior of $F(Q, t)$ for t in the β -relaxation regime. $A(Q)$ is the third quantity that we can calculate from the experimental analysis. The Lamb-Mössbauer factor, traditionally called f_Q^{inc} , behaves similarly to the vibrational Debye-Waller factor. As a matter of fact, we find that it can be expressed as

$$A(Q) = f_Q^{inc} = \exp(-\langle a^2 \rangle Q^2 / 3), \quad (15)$$

where a plays the role of the cage radius. Thus, also the radius of the cage can be found through QENS. From our MD study we found that the radius of the cage $\langle a \rangle$ decreases from 0.45 Å for $T=284.5$ K to 0.38 Å for the lowest temperature investigated, namely, $T=206.3$ K. The temperature dependence of $\langle a^2 \rangle$ is consistent with a linear law, as expected for harmonic dynamics. We also note that this radius is of the same order of magnitude of typical radii of cages measured in other liquids [49].

In Fig. 15 we show, respectively, $S(Q, t)$ obtained as a Fourier transform of the fit to the center of mass as a function of T at Q_{max} and as a function of Q for $T=213.6$ K on a semilogarithmic scale. We observe that as T increases the inelastic intensity increases and the quasielastic intensity decreases. Below T_C there would be a huge transfer of intensity from the elastic to the inelastic part of the spectrum, a direct consequence of the increase of the plateau level in $F(Q, t)$, with decreasing T . Above T_C , where our simulation has been performed, this phenomenon is much weaker but still persistent. Close to Q_{max} the $A(Q)$ extracted from the fit of

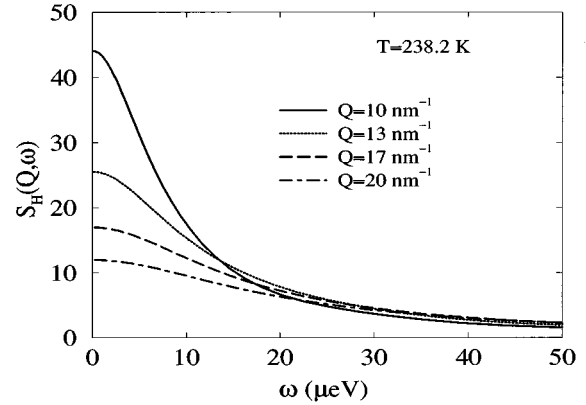


FIG. 16. Fourier transform of the hydrogen density autocorrelation function calculated from MD data for $Q=1, 1.33, 1.66,$ and 2 \AA^{-1} .

Eq. (13) to MD data decreases in fact from 0.851 at $T=206.3$ K to 0.778 at $T=284.5$ K.

The experimental test of MCT with QENS on water is limited not only by the nucleation temperature but also by the resolution of the experimental apparatus. In Fig. 16 we show the same function on a linear scale for a state point slightly below the temperature of density maximum for SPC/E. We see that in order to test the MCT of supercooled water one needs to use an experimental resolution of at least $10 \mu\text{eV}$ and to supercool as much as possible. High resolutions can nowadays be achieved in the high-resolution machines of several neutron facilities and with the next generation of machines we expect the resolution to improve further.

In summary, given the present analysis, we believe that with the best instrumental resolution available the following prediction of MCT can be tested by QENS on supercooled water: (a) the behavior of the Lamb-Mössbauer factor $A(Q)$, (b) the hydrogen relaxation times $\tau(Q, t)$, and (c) the stretched exponent $\beta(Q, t)$ of the late α region. We cannot conclude whether the range of validity of the b region is sufficient to get it from the slope of $S(Q, t)$.

VI. MCT ANALYSIS OF THE RESPONSE FUNCTION

In this section we analyze the behavior of the single-particle imaginary part $\chi''(\omega, Q)$ of the dynamics susceptibility $\chi(\omega, Q)$ for SPC/E water. This quantity is, in the classical limit, the time Fourier transform of $F(Q, t)$ multiplied by ω . The dynamic susceptibility can therefore be easily extracted from neutron-scattering experiments.

The predictions of MCT about the behavior of this function are the Fourier transforms of the predictions of the theory in (Q, t) space. Nonetheless, some of the features of MCT are more evident if presented in terms of χ'' . In particular, the α relaxation, which is the one on which we focused mostly in this paper, is clearly sketched. From the detailed test of MCT for SPC/E water in (Q, t) space [15] we know what predictions the χ'' of SPC/E supercooled water has in common with an ideal MCT-like liquid. We show the shape of χ'' and summarize it in the following for the sake of a future comparison with experimental data.

According to MCT, χ'' displays two peaks. These peaks correspond to the two-step relaxation scenario.

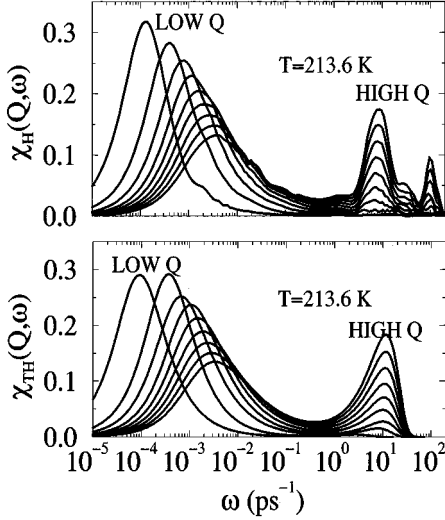


FIG. 17. On the top $\chi''_H(Q, \omega)$ for $T=213.6$ K and Q values as integer multiples of 0.33. Lower Q are on the bottom. These curves have been obtained from direct Fourier transform of $F_H(Q, t)$. A stretched exponential tail with the relaxation time extracted with the fit has been added. On the bottom the same correlators obtained from the Fourier transform of the formula we used to fit $T(Q, t)$ [Eq. (13)].

The prediction of MCT for the behavior with T of the position of the frequency corresponding to the first maximum ω_{max} is fulfilled by our data since

$$\omega_{max} \sim \tau_l^{-1} \sim (T - T_c)^\gamma. \quad (16)$$

The χ'' obtained by direct Fourier transform of MD data are, generally speaking, quite difficult to obtain because they extend for several decades in time or frequency. For this reason, before Fourier transforming the intermediate scattering function, we smoothed them with a spline under tension [50], in analogy with the procedure used in Ref. [51]. The results of this procedure, although still not completely free from irregularities, allow us to see the differences between the Fourier transform of our MD data calculated for the hydrogen atom trajectories and the Fourier transform of the formula we use to fit the correlator of the center of mass in (Q, t) space [Eq. (13)]. We perform here this comparison in order to further test the possibility to use the Fourier transform of our formula to fit the QENS data. In Fig. 17, top, we show the χ''_H obtained from the Fourier transform of our MD data for $T=213.6$ K at all the Q investigated. In Fig. 17, bottom, we show exactly the same correlators as in Fig. 16 except these are calculated from the Fourier transform of Eq. (13) and the parameters of the fit to $T(Q, t)$. We do see that the main features of the MD curves are well reproduced by the Fourier transform of our fit, in particular, the intensity and the position of the two main peaks. The main differences between these two figures are in the extremely high-frequency region, which is beyond the QENS range. In Fig. 18 we show the behavior of the same correlator as a function of T at Q_{max} .

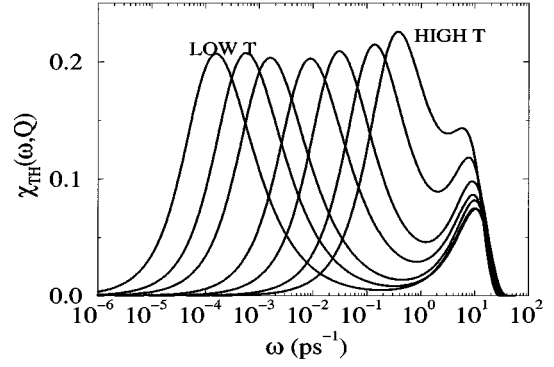


FIG. 18. $\chi''_{TH}(Q, \omega)$ calculated as in Fig. 17, bottom, for all the investigated temperatures at Q_{max} . The α peak of the lower temperatures is more on the left.

VII. CONCLUSION

In this paper we have analyzed the possibility of detecting the dynamic slowing down near T_C predicted by MCT in supercooled water using QENS. The analysis has been carried out by using a set of MD data on supercooled SPC/E water obtained by sufficiently long simulations, which allowed us to confirm the existence of the α relaxation. SPC/E water manifests a typical MCT behavior analyzed in detail in our previous papers [14,15]. We have discussed the ability of the SPC/E potential to mimic properties of real water. The result, though encouraging, cannot be considered definitive. Although SPC/E appears to be a good potential for pressures and temperatures close to ambient, it is likely that the computed properties of the SPC/E water begin to deviate from those of the real water when it is deeply supercooled. Nevertheless, the prediction that the kinetic glass transition exists in water is a worthwhile point to test experimentally. QENS for supercooled water is the best way for testing the MD results of SPC/E water. Due to a lack of high-resolution QENS data in the supercooled region, a direct comparison between QENS and MD data cannot be performed at this time. Therefore, another QENS experiment specifically designed to test the SPC/E predictions would be very valuable. In this paper, therefore, we use the accurate MD data to test quantitatively the accuracy of various approximations used in analyzing QENS data of water in the past. Taking advantage of the possibility of calculating exactly the ‘‘self’’ part of all the $F(Q, t)$ of the system, namely, $F_H(Q, t)$, $R(Q, t)$, $T(Q, t)$, and $F_O(Q, t)$, we test the range of validity of a set of approximations: the decoupling of $R(Q, t)$ and $T(Q, t)$, the jump-diffusion approximation for the translational part, and the rotational-diffusion approximation for the rotational part.

QENS probes directly the dynamics of single-particle motions of hydrogen atoms in water. In principle, the dynamics of hydrogen motion is affected by the translation as well as the rotation of the molecule. We first showed that $F_H(Q, t)$ decays to zero similarly to $T(Q, t)$. Both display a typical MCT scenario, namely, a two-step decay in time, with the long-time α relaxation characterized by a stretched exponential function.

In the lower part of the available Q range of a typical high-resolution QENS experiment, from 0.2 up to 0.5 \AA^{-1} , the rotational-translational coupling appears to be quite neg-

ligible since $R(Q,t) \sim 1$. Therefore, in this region $F_H(Q,t) \sim T(Q,t)R(Q,t) \sim T(Q,t)$. It is not, however, negligible in the high- Q region, close to the peak of the structure factor, covered in a typical low-resolution QENS experiment, for all the investigated temperatures. On the other hand, at extremely long times in the supercooled region, the effect of the coupling and the decay of the rotational correlation function tend to cancel each other so that $F_H(Q,t) \sim T(Q,t)$ also in this region.

The maximum of the correlator describing the rotational-translational coupling $F_{con}(Q,t)$ scales like D with temperature. Furthermore, the $R(Q,t)$ decays on the same time scale as the $T(Q,t)$ at a certain value of Q . These phenomena indicate that the time dependence of the rotational part of the correlation function is also completely synchronized with the breaking and reforming of cages in the liquid. When the cages begin to relax the molecule is free to move and rotate and the correlation function decouples in the product of $R(Q,t)$ and $T(Q,t)$ and decays to zero.

The direct consequence of $F_H(Q,t) \sim T(Q,t)$ for long times at all Q is that in QENS no signatures of rotation can be detected in the supercooled region and experimental data can be analyzed in terms of the translational part of the dynamics alone. This implies that a high-resolution QENS spectrum can be fitted with the Fourier transform of Eq. (13). This procedure allows one to extract the strength factor, the Lamb-Mössbauer factor, the relaxation time τ , and the stretch exponent of the α relaxation, β . By employing a high-resolution time-of-flight spectrometer and supercooling water down to the lowest experimentally accessible temperature (about -20°C), a QENS experiment should be capable of detecting MCT signatures in water. For SPC/E supercooled water close to Q_{max} , the previously often used jump-diffusion and the rotational-diffusion approximations are not accurate. In fact, we showed that Sears expansion is accurate (see Fig. 11), but the various $C_l(Q)$ do not decay in an exponential fashion, as a rotational-diffusion model would

require. We also showed that a jump-diffusion analysis of the HWHM of the $S_H(Q,t)$ would mask a possible stretch exponential behavior.

We would like to conclude this paper by noting that the picture of water behaving like a typical glass former undergoing a kinetic glass transition can be reconciled with the “traditional” picture of dynamics of water. In fact, in many occasions in the past, the dynamics of water has been analyzed in terms of models based on the formation and breaking of hydrogen bond cages [40]. It is considered realistic that the translational diffusion of water is possible only by first activating the rotation that switches the hydrogen bonding [52]. Through the slow process of bond switching, molecules change their neighborhood and diffuse. The strong-hydrogen-bond interaction is responsible for the formation of strong cages even if the local number density is much smaller than in simple liquids, where packing controls the process of cage formation and stability. The hydrogen-bond network, instead of destroying the tendency toward a MCT-like behavior, would then trigger it. The strong-hydrogen-bonded cage does not allow for molecular rotations within the cage. Indeed, the molecular correlations display a two-step process. On the fast-time scale the molecule performs hindered rotations within the cage, while on a long-time scale they diffuse and rotate. Thus the process of changing the hydrogen-bond pattern is realized by a strongly coupled rototranslational motion. A theoretical model to describe such motion would be very valuable for the correct interpretation of the T and Q dependence of neutron data.

ACKNOWLEDGMENTS

The research of S.H.C. was funded by the Division of Materials Sciences of the U.S. Department of Energy. P.G. acknowledges financial support from the Foundation Blanciflor Boncompagni-Ludovisi. The research of F.S. and P.T. was supported by GNSM/CNR and INFN/MURST.

-
- [1] D. Di Cola, A. Deriu, M. Sampoli, and A. Torcini, *J. Chem. Phys.* **104**, 4223 (1996).
 - [2] A. Cunsolo and M. Nardone, *J. Chem. Phys.* **105**, 3911 (1996).
 - [3] M. Matsumoto and I. Ohmine, *J. Chem. Phys.* **104**, 2705 (1996).
 - [4] D. Paschek and A. Geiger (unpublished).
 - [5] P. G. Debenedetti, *Metastable Liquids: Concepts and Principles* (Princeton University Press, Princeton, 1997).
 - [6] A. P. Sokolov, J. Hurst, and D. Quitmann, *Phys. Rev. B* **51**, 12 865 (1995).
 - [7] G. E. Walrafen and Y. C. Chu, *J. Phys. Chem.* **99**, 11 225 (1995).
 - [8] D. Bertolini and A. Tani, *Phys. Rev. E* **52**, 1699 (1995).
 - [9] N. Karger, H.-D. Lüdemann, and M. G. Sceats, *Ber. Bunsenges. Phys. Chem.* **99**, 1104 (1995).
 - [10] D. Bertolini and A. Tani, *Phys. Rev. E* **51**, 1091 (1995).
 - [11] H. Weingärtner, R. Haselmeier, and M. Holz, *J. Phys. Chem.* **100**, 1303 (1996).
 - [12] R. J. Speedy and C. A. Angell, *J. Chem. Phys.* **65**, 851 (1976).
 - [13] For a critical review see F. Sciortino, in *The Physics of Complex Systems*, Proceedings of the International School of Physics “Enrico Fermi,” Course CXXXIV, Varenna, 1996, edited by F. Mallamace and H. E. Stanley (IOS, Amsterdam, 1997).
 - [14] P. Gallo, F. Sciortino, P. Tartaglia, and S.-H. Chen, *Phys. Rev. Lett.* **76**, 2730 (1996).
 - [15] F. Sciortino, P. Gallo, P. Tartaglia, and S.-H. Chen, *Phys. Rev. E* **54**, 6331 (1996).
 - [16] E. Leuthesser, *Phys. Rev. A* **29**, 2765 (1984); U. Bengtzelius, W. Götze, and A. Sjölander, *J. Phys. C* **17**, 5915 (1984).
 - [17] S. Sastry, P. G. Debenedetti, F. Sciortino, and H. E. Stanley, *Phys. Rev. E* **53**, 6144 (1996).
 - [18] F. X. Prielmeir, E. W. Lang, R. J. Speedy, and H.-D. Lüdemann, *Phys. Rev. Lett.* **59**, 1128 (1987); F. X. Prielmeir, E. W. Lang, R. J. Speedy, and H.-D. Lüdemann, *Ber. Bunsenges. Phys. Chem.* **92**, 1111 (1988).
 - [19] C. A. Angell, *Nature (London)* **331**, 206 (1988).
 - [20] B. N. Brockhouse, *Nuovo Cimento Suppl.* **9**, 45 (1958); *Phys. Rev. Lett.* **2**, 287 (1959).

- [21] M. Sakamoto, B. N. Brockhouse, R. G. Johnson, and N. K. Pope, *J. Phys. Soc. Jpn.* **17**, 370 (1962).
- [22] S.-H. Chen, J. Teixeira, and R. Nicklow, *Phys. Rev. A* **26**, 3477 (1982).
- [23] J. Teixeira, M.-C. Bellissent-Funel, S.-H. Chen, and A. J. Dianoux, *Phys. Rev. A* **31**, 1913 (1985).
- [24] F. Cavatorta, A. Deriu, D. Di Cola, and H. D. Middendorf, *J. Phys.: Condens. Matter* **6**, A113 (1994).
- [25] In this context we will refer to the Debye-Waller factor for the delocalization of the vibrational motion.
- [26] C. T. Chudley and R. J. Elliot, *Proc. Phys. Soc. London* **77**, 353 (1966).
- [27] V. F. Sears, *Can. J. Phys.* **45**, 237 (1967).
- [28] J. J. Ullo, *Phys. Rev. A* **36**, 816 (1987).
- [29] H. J. C. Berendsen, J. R. Grigera, and T. P. Straatsma, *J. Phys. Chem.* **91**, 6269 (1987).
- [30] J. Brodholt and B. Wood, *J. Geophys. Res.* **98**, 519 (1993).
- [31] Y. Guissani and B. Guillot, *J. Chem. Phys.* **98**, 8221 (1993).
- [32] P. E. Smith and Wilfred. F. van Gunsteren, *Chem. Phys. Lett.* **215**, 315 (1993).
- [33] L. A. Baez and P. Clancy, *J. Chem. Phys.* **101**, 9837 (1994).
- [34] P. H. Poole, F. Sciortino, U. Essmann, and H. E. Stanley, *Nature (London)* **360**, 324 (1992).
- [35] P. H. Poole, F. Sciortino, U. Essmann, and H. E. Stanley, *Phys. Rev. E* **48**, 3799 (1993).
- [36] A. Soper, *Chem. Phys.* **88**, 187 (1984); A. K. Soper and M. G. Phillips, *ibid.* **107**, 47 (1986).
- [37] W. E. Thiessen and A. H. Narten, *J. Chem. Phys.* **77**, 2656 (1982).
- [38] For further details on our findings see Refs. [14,15] and for a review on MCT theories see Refs. [16,39].
- [39] W. Götze and L. Sjögren, *Rep. Prog. Phys.* **55**, 241 (1992).
- [40] S.-H. Chen, in *Hydrogen Bonded Liquids*, Vol. 329 of *NATO Advanced Study Institute, Series C: Mathematical and Physical Sciences*, edited by J. C. Dore and J. Teixeira (Kluwer Academic, Dordrecht, 1991).
- [41] See for example, C. A. Angell, *Science* **267**, 1924 (1995).
- [42] L. J. Lewis and Göran Wahnström, *Phys. Rev. E* **50**, 3865 (1994).
- [43] J. Horbach, W. Kob, K. Binder, and C. A. Angell, *Phys. Rev. E* **54**, R5897 (1996).
- [44] F. Sciortino and P. Tartaglia, *Phys. Rev. Lett.* **78**, 2385 (1997).
- [45] The time dependence of $b(t)$ is independent from the choice of the reference system. In the reference system defined by the molecule center of mass $\mathbf{R}(t)$, all mixed correlation functions are zero.
- [46] The two dipole moment autocorrelation functions $C_1(t)$ and $C_2(T)$ are reported respectively in Figs. 22 and 23 of Ref. [15] together with the fit to a stretched exponential. The parameters extracted from the fit are reported in Table II of Ref. [15] and the discussion is carried out in Sec. IV E of the same paper. See also F. Sciortino, S. H. Chen, P. Gallo, and P. Tartaglia, in *Structure and Dynamics of Glasses and Glass Formers*, edited by C. A. Angell, T. Egami, J. Kieffer, U. Nichhaus, and K. L. Ngai, MRS Symposia Proceedings No. 455 (Materials Research Society, Pittsburgh, 1997).
- [47] T. Keyes, *J. Chem. Phys.* **104**, 9349 (1996).
- [48] R. Kubo, *J. Phys. Soc. Jpn.* **12**, 570 (1957).
- [49] See, for example, W. Petry, E. Bartsch, F. Fujiara, M. Kiebelm, H. Sillescu, and B. Farago, *Z. Phys. B* **83**, 175 (1991).
- [50] C. H. Reinsch, *Numer. Math.* **10**, 177 (1967).
- [51] W. Kob and H. C. Andersen, *Phys. Rev. E* **51**, 4626 (1995); **52**, 4134 (1995).
- [52] F. Sciortino, A. Geiger, and H. E. Stanley, *Nature (London)* **354**, 218 (1991); F. Sciortino, A. Geiger, and H. E. Stanley, *J. Chem. Phys.* **96**, 3857 (1992).